An Iron-Activated Citrate Transporter, MtMATE67, Is Required for Symbiotic Nitrogen Fixation[1][OPEN]

Igor S. Kryvoruchko,[a,2,3] Pratyush Routray,[b,2] Senjuti Sinharoy,[a,2,4] Ivone Torres-Jerez,[a] Manuel Tejada-Jiménez,[c] Lydia A. Finney,[d] Jin Nakashima,[a] Catalina I. Pislariu,[a,5] Vagner A. Benedito,[e] Manuel González-Guerrero,[c] Daniel M. Roberts,[b] and Michael K. Udvardi[a,6]

[a]Noble Research Institute, Ardmore, Oklahoma 73401
[b]Department of Biochemistry and Cellular and Molecular Biology, University of Tennessee, Knoxville, Tennessee 37996
[c]Centro de Biotecnología y Genómica de Plantas (UPM-INIA), Universidad Politécnica de Madrid, Madrid 28223, Spain
[d]Argonne National Laboratory, Argonne, Illinois 60439
[e]Division of Plant and Soil Sciences, West Virginia University, Morgantown, West Virginia 26506

ORCID IDs: 0000-0003-3636-1732 (I.S.K.); 0000-0003-2323-2587 (S.S.); 0000-0003-1702-6015 (M.T.-J.); 0000-0002-2131-7651 (V.A.B.); 0000-0001-7334-5286 (M.G.-G.); 0000-0002-0780-7056 (D.M.R.); 0000-0001-9850-0828 (M.K.U.).

Iron (Fe) is an essential micronutrient for symbiotic nitrogen fixation in legume nodules, where it is required for the activity of bacterial nitrogenase, plant leghemoglobin, respiratory oxidases, and other Fe proteins in both organisms. Fe solubility and transport within and between plant tissues is facilitated by organic chelators, such as nicotianamine and citrate. We have characterized a nodule-specific citrate transporter of the multidrug and toxic compound extrusion family, MtMATE67 of *Medicago truncatula*. The MtMATE67 gene was induced early during nodule development and expressed primarily in the invasion zone of mature nodules. The MtMATE67 protein was localized to the plasma membrane of nodule cells and also the symbiosome membrane surrounding bacteroids in infected cells. In oocytes, MtMATE67 transported citrate out of cells in an Fe-activated manner. Loss of *MtMATE67* gene function resulted in accumulation of Fe in the apoplasm of nodule cells and a substantial decrease in symbiotic nitrogen fixation and plant growth. Taken together, the results point to a primary role of MtMATE67 in citrate efflux from nodule cells in response to an Fe signal. This efflux is necessary to ensure Fe(III) solubility and mobility in the apoplasm and uptake into nodule cells. Likewise, MtMATE67-mediated citrate transport into the symbiosome space would increase the solubility and availability of Fe(III) for rhizobial bacteroids.

Symbiotic nitrogen fixation (SNF) by rhizobia in legume root nodules injects around 40 million tons of nitrogen into agricultural systems every year in a natural and sustainable way (Peoples et al., 2009). A series of chemical and physical interactions between rhizobia bacteria from the soil and legume root cells result in dedifferentiation and division of plant cells to form a nodule primordium and colonization of plant cells via an "infection thread" that delivers rhizobia into cortical cells (Murray, 2011). Rhizobia are taken into host cells via endocytosis, which engulfs the bacteria in a plant membrane called the symbiosome membrane (SM) and forms a novel "organelle," the symbiosome (Udvardi and Poole, 2013). Bacteria within symbiosomes grow and divide until infected cells are packed with thousands of symbiosomes containing one or a few bacteria each, depending on the plant species (Maróti and Kondorosi, 2014). Oxygen concentrations around rhizobia plummet during nodule development, through a combination of restricted gas diffusion across the outer cell layers of the nodule, high rates of respiration by plant mitochondria and rhizobia, and binding and rapid delivery of oxygen by leghemoglobin to support respiration (Appleby, 1984; Ott et al., 2005). Low-oxygen concentration in infected nodule cells contributes to the differentiation of rhizobia into nitrogen-fixing bacteroids and enables prolonged activity of oxygen-labile nitrogenase (Hennecke, 1990).

Legume species form either determinate nodules with a temporary meristem that produces a spherical organ or indeterminate nodules with persistent meristems that give rise to cylindrical or coralloid organs. Both nodule types feature a central infected zone, composed of both infected and uninfected cells, surrounded by several layers of uninfected cells (Oldroyd, 2013). The persistent meristem of indeterminate nodules generates a developmental gradient of cells that form four zones: meristem (zone I); invasion zone (II) in which rhizobia colonize plant cells, proliferate, and differentiate; the nitrogen-fixation zone (III) where bacteroids produce ammonia for the plant; and the senescence zone (IV), which is present only in older nodules and may serve to recycle nutrients (Vasse et al., 1990).

Iron (Fe) plays central roles in SNF as a cofactor essential for the function of multiple proteins including:

the two subunits (the Fe-protein and Fe-Mo protein) of the nitrogen-fixing enzyme, nitrogenase; plant and bacterial cytochromes required for respiration and energy metabolism; leghemoglobin to transport oxygen and buffer free molecular oxygen at nanomolar concentrations compatible with activity of oxygen-labile nitrogenase; and a variety of other Fe-proteins such as ferredoxins and hydrogenases (Tang et al., 1990; Brear et al., 2013). Insufficient Fe in the soil or growth medium limits SNF (Tang et al., 1990; O'Hara, 2001), and mutation of a plant Fe transporter, MtNramp1, also compromises SNF (Tejada-Jiménez et al., 2015). Based on x-ray fluorescence data from *Medicago truncatula*, Fe appears to be delivered into nodules via the vascular system and released into the apoplasm of cells in the invasion zone before being taken up by plant cells and transported to bacteroids (Rodríguez-Haas et al., 2013). However, our knowledge of the molecular mechanisms of Fe transport between and within cells of nodules is far from complete.

Fe has poor solubility and high oxidizing power (Conte and Walker, 2011). Excessive free Fe, especially Fe(II), is toxic because it can generate highly damaging hydroxyl radicals via the Fenton reaction (Jeong and Guerinot, 2009). To avoid accumulation of free Fe, and precipitation of Fe salts, citrate, and nicotianamine are commonly used to chelate Fe inside plants, which also facilitates Fe transport (Kobayashi and Nishizawa, 2012). Fe is translocated within the xylem as a ferric (Fe-III) citrate complex (Brüggemann et al., 1993; Rellán-Alvarez et al., 2010).

Several different families of transporters have been implicated in Fe movement in plants, including YSL (Yellow Stripe-Like), Zinc-Iron Permease, NRAMP (Natural Resistance Associated Macrophage Protein), and VIT (Vacuolar Iron Transporter) proteins that transport Fe across membranes (Curie et al., 2009; Jeong and Guerinot, 2009; Conte and Walker, 2011; Brear et al., 2013), as well as MATE (Multidrug And Toxic-compound Extrusion) proteins that transport citrate, which helps to mobilize Fe (Omote et al., 2006; Takanashi et al., 2014). YSL proteins transport both Fe(II) and Fe(III) chelated to NA into the phloem or sink cells (Curie et al., 2009). Soybean (*Glycine max*) divalent metal transporter 1, GmDMT1, is an NRAMP family member located on the soybean SM that transports Fe(II) and possibly zinc and manganese (Kaiser et al., 2003). It is unclear whether its main role is uptake or efflux of Fe from the symbiosomes. MtNRAMP1 is located on the plasma membrane (PM) of *M. truncatula* nodule cells, where it is required for Fe uptake and effective SNF (Tejada-Jiménez et al., 2015). *Lotus japonicus LjSEN1* is a member of the VIT family and is required for SNF in Lotus nodules (Hakoyama et al., 2012). By analogy to vacuolar Fe transporters, LjSEN1 may be involved in Fe transport into symbiosomes, although the intracellular location and substrate specificity of the protein remain to be determined. LjMATE1 of *L. japonicus* is a citrate transporter involved in Fe homeostasis and SNF in nodules (Takanashi et al., 2013). However, lack of information about its intracellular location clouds its physiological role.

We have investigated a nodule-induced MATE transporter of *M. truncatula*, MtMATE67, and found that the protein transports citrate in an Fe-activated manner. We localized the protein in the PM of cells primarily at the distal end of nodules where Fe is delivered from the root via vascular bundles. Furthermore, we found that *M. truncatula mate67* mutants are impaired in SNF. These and other results presented here point to a key role of MtMATE67 in Fe uptake into nodule cells and are discussed in the context of Fe homeostasis for symbiotic nitrogen fixation.

RESULTS

MtMATE67 Is Induced during Nodule Development

Using the *M. truncatula* Gene Expression Atlas (MtGEA; Benedito et al., 2008), we identified a putative MATE transporter gene, *Medtr8g037170* (corresponding to Affymetrix probeset, Mtr.3624.1.S1_at) that was induced 205-fold in mature nodules compared to roots (Supplemental Fig. S1). We named this gene *MtMATE67*, to follow the consecutive numbering of *M. truncatula* MATE transporters published recently

[1] This work was supported by the U.S. Department of Agriculture, Agriculture and Food Research Initiative Program (grant no. 2010-65115-20384) and the National Science Foundation Plant Genome Research Program (IOS1127155) and Major Research Instrumentation Program (grants IOS-1127155 and DBI-0722635). Financial support for D.M.R.'s laboratory came from the National Science Foundation (grant no. MCB-1121465). Work at M.G.-G.'s lab was funded by the European Research Council Starting Grant Program (grant no. ERC-2013-StG-335284). Use of the Advanced Photon Source facility was supported by the U.S. Department of Energy (under contract no. DE-AC02-06CH11357).

[2] These authors contributed equally to the article.

[3] Current address: Department of Molecular Biology and Genetics, Bogazici University, Istanbul 34342, Turkey.

[4] Current address: National Institute of Plant Genome Research, Aruna Asaf Ali Marg, New Delhi 110067, India.

[5] Current address: Department of Biology, Texas Woman's University, 304 Administration Dr., Denton, Texas 76204.

[6] Address correspondence to mudvardi@noble.org.

The author responsible for distribution of materials integral to the findings presented in this article in accordance with the policy described in the Instructions for Authors (www.plantphysiol.org) is: Michael Udvardi (mudvardi@noble.org).

I.K., P.R., S.S., M.G.-G., V.A.B., D.R., and M.K.U. contributed to the experimental design; I.K., S.S., I.T.-J., P.R., M.T.-J., M.G.-G., L.F., C.I.P., and J.N. were involved in the experimental work; P.R. performed transport assays in *Xenopus laevis* oocytes; M.T.-J. generated confocal immunolocalization images; L.F. and M.G.-G. collected the data on Fe distribution in nodules; C.I.P. provided data on transcriptional profiling of nodule developmental zones; J.N. conducted transmission electron microscopy; I.K., S.S., I.T.-J., P.R., and M.G.-G. were responsible for the data analysis; I.K., S.S., and M.K.U. wrote the manuscript.

[OPEN] Articles can be viewed without a subscription.

www.plantphysiol.org/cgi/doi/10.1104/pp.17.01538

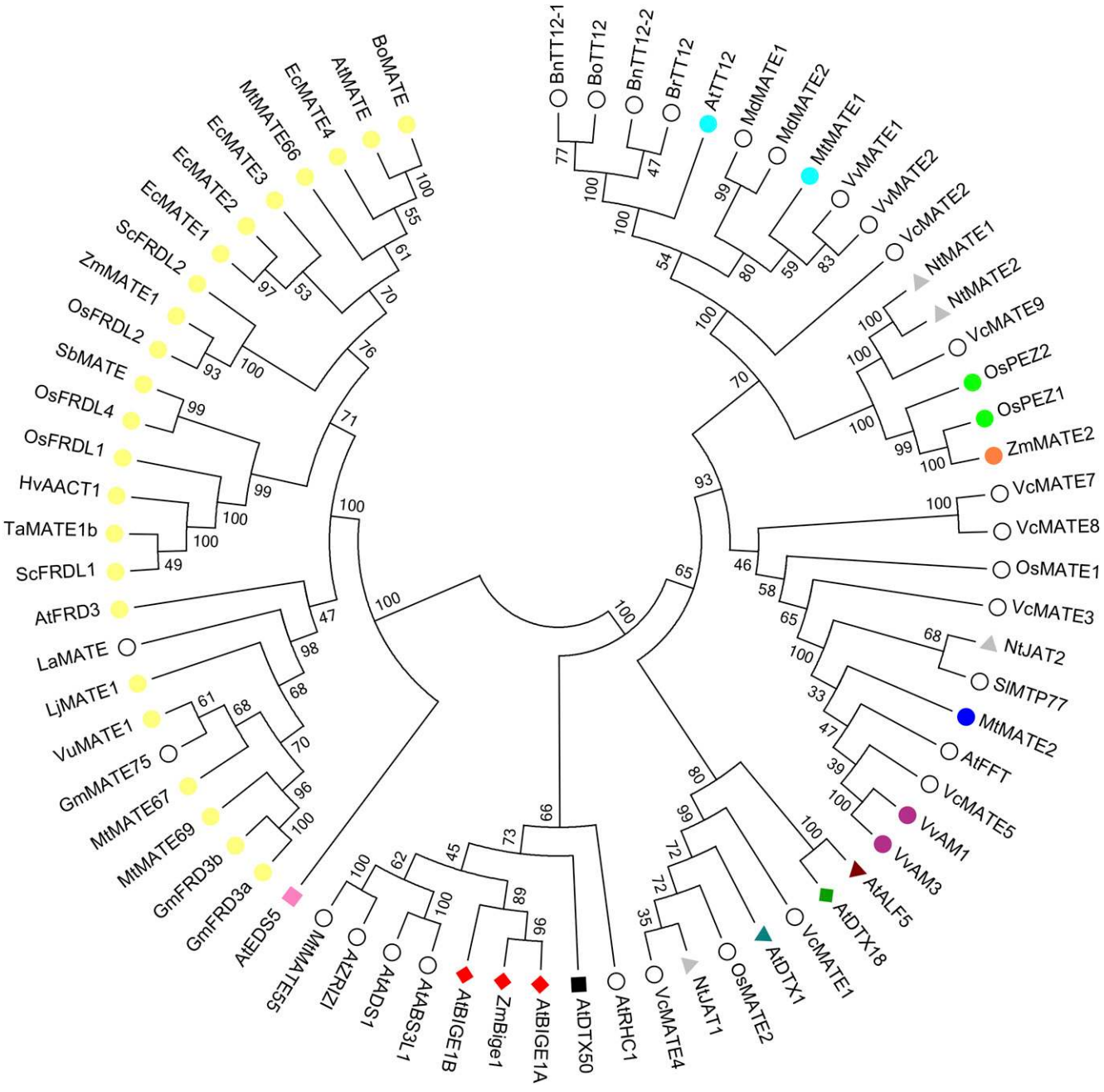

Figure 1. Bootstrap consensus maximum parsimony tree of 70 published plant MATE transporters. The tree was constructed with MEGA7.0.21, using protein sequences from GenBank (default), UniProtKB/TrEMBL database (NtJAT1), and Genoscope database (VvMATE1 and VvMATE2), which were manually trimmed from N terminus and C terminus to a consensus sequence before the alignment. The original alignment file is available as Supplemental Data Set S3. Tree branch values are bootstrap values (1,000 reiterations). Transporters are color-labeled according to their substrate (Supplemental Table S1): yellow circle, citrate; white circle, substrate unknown; turquoise circle, cyanidin-3-*O*-glucoside; gray pyramid, nicotine; light green circle, protocatechuic acid; orange circle, anion; blue circle, malonylated flavonoid glucosides; purple circle, acylated anthocyanins; brown inverted pyramid, tetramethylammonium; green diamond, hydroxycinnamic acid amide; darkcyan inverted pyramid, norfloxacin; black square, abscisic acid (ABA); red diamond, signaling molecule; pink square, salicylic acid (SA).

(Wang et al., 2017). In *M. truncatula*, the MATE family consists of at least 70 members (*Medicago* genome, IMGAG version 4; Tang et al., 2014). Phylogenetic analysis of all 70 published plant MATE transporters (see Supplemental Table S1 for references) placed MtMATE67 into a clade together with *L. japonicus* LjMATE1 and Arabidopsis (*Arabidopsis thaliana*) AtFRD3, both citrate efflux carriers (Fig. 1; Durrett et al., 2007;

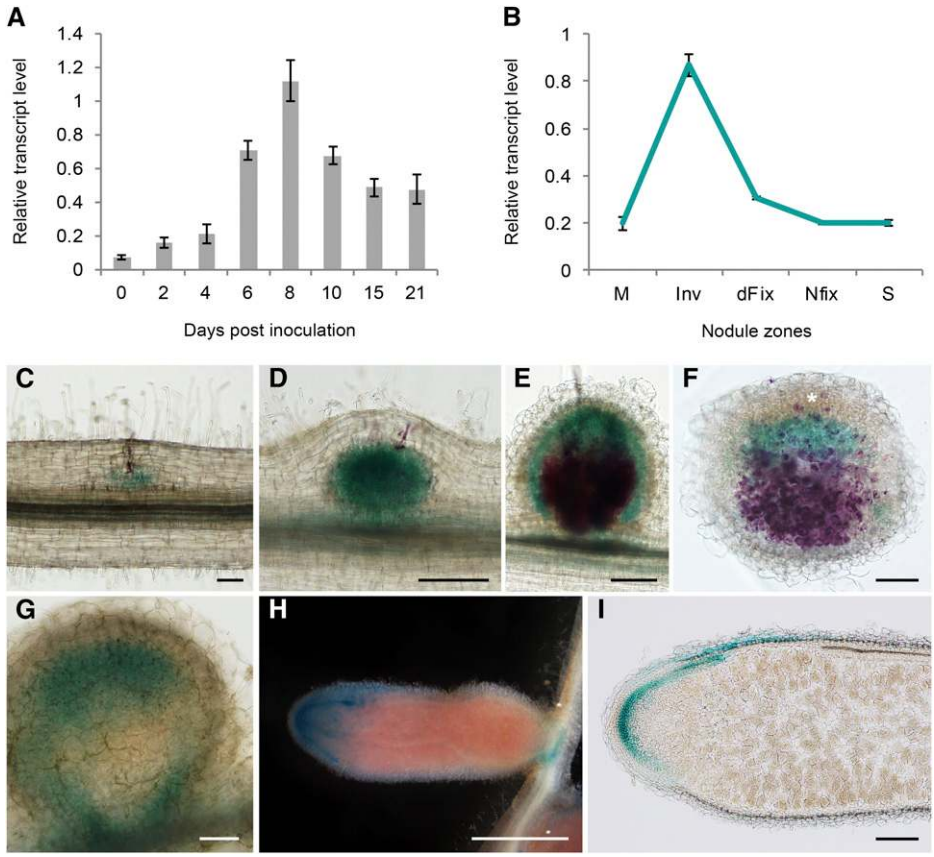

Figure 2. Nodule-specific expression of *MtMATE67* is limited to the meristem, distal invasion zone, and vascular bundles of the nodule tip. A, Time course of *MtMATE67* expression in nodules of ecotype R108 performed using qRT-PCR. B, Expression profiling (qRT-PCR) of *MtMATE67* in manually dissected nodule zones of a mature nodule from ecotype A17 (28 dpi). Error bars in A and B represent SD values of three biological replicates. Nodule zones: M, meristem; Inv, invasion zone; dFix, distal nitrogen-fixation zone; Nfix, nitrogen-fixation zone; S, senescence zone. C to I, X-Gluc staining for *MtMATE67* (ecotype A17) promoter activity (G–I) or double-staining using Magenta-Gal and X-Gluc (C–F) for simultaneous visualization of *MtMATE67* expression (blue) and *S. meliloti* colonization (purple). C, Dividing cortical cells. D, Nodule primordium (4 dpi). E, Young nodule (10 dpi). F, A 50-μm longitudinal microtome section of a 10-dpi nodule. Asterisk indicates the nodule meristem. G, Young nodule (10 dpi) without Magenta-Gal staining. H, Mature nodule (38 dpi) after 6-h staining for GUS activity. I, A 50-μm microtome section of a mature nodule (38 dpi) after 1-h staining for GUS activity. Bars = 100 μm in C to G, 1,000 μm in H, and 200 μm in I.

Roschzttardtz et al., 2011; Takanashi et al., 2013). Like *MtMATE67* (Supplemental Fig. S1), *LjMATE1* is also expressed in a nodule-specific manner (Takanashi et al., 2013). Similar to most MATE transporters from all kingdoms (Omote et al., 2006), MtMATE67 has 12 predicted transmembrane domains (Supplemental Fig. S2).

To extend the *MtMATE67* gene expression data from MtGEA, we measured transcript levels of this gene in roots and in nodules of genotypes A17 (the genomic reference) and R108 (parent genotype of our *Tnt1*-insertion mutant population) at different stages of development and in distinct nodule zones, using qRT-PCR. *MtMATE67* relative transcript levels were very low in wild-type roots before inoculation. Transcript levels increased steadily after inoculation with rhizobia between 2 and 8 d postinoculation (dpi), reaching levels 15-fold higher than in 0 dpi roots and declined slightly thereafter (Fig. 2A). To reveal the spatial pattern of *MtMATE67* expression, we performed qRT-PCR analysis on nodule zones of 28 dpi nodules from ecotype A17. *MtMATE67* transcripts were detected in all nodule zones with peak expression in the invasion zone (Fig. 2B).

To confirm and extend the spatio-temporal nodule expression data obtained by qRT-PCR, we generated a *pMATE67:GUS* promoter-reporter construct bearing 2,928 bp of the *MtMATE67* promoter sequence of ecotype A17 fused to the *GUS* gene, which was introduced into *M. truncatula* roots by "hairy" root transformation (Fig. 2, C–I). In addition to GUS staining, tissue sections were stained with Magenta-Gal to visualize *lacZ*-expressing rhizobia (Fig. 2, C–F). During *M. truncatula* nodule primordium formation, cell division initiates in the inner cortex and in the pericycle below the activated cortical cells (Timmers et al., 1999). In our samples, GUS staining was detected within dividing cells of the

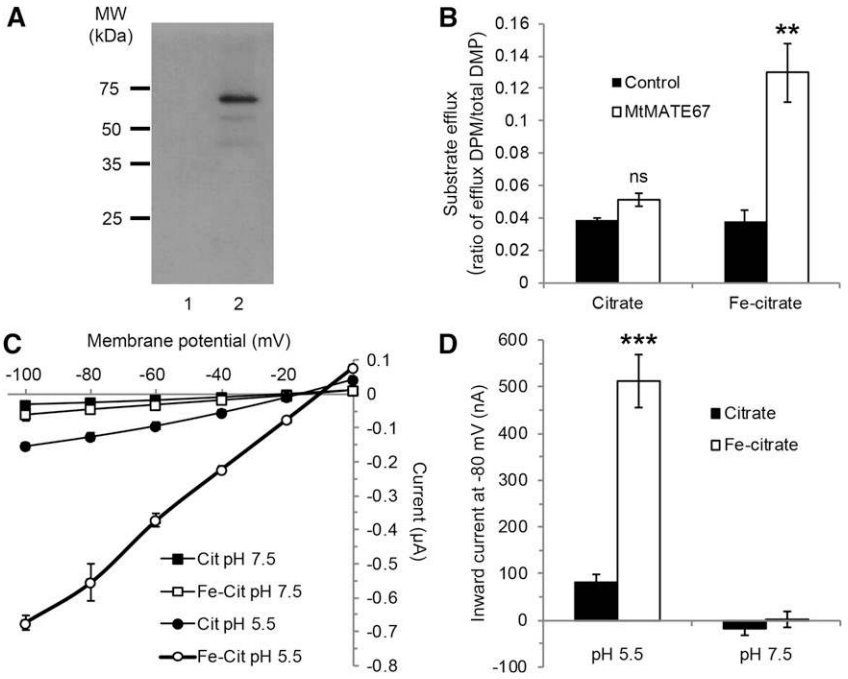

Figure 3. Citrate efflux activity of MtMATE67 in *X. laevis* oocytes. A, Anti-FLAG tag western-blot analysis of *X. laevis* oocytes microinjected with sterile water (control; 1) or *MtMATE67* cRNA with a C-terminal FLAG tag (2). B, Radiolabeled [^{14}C]-citrate efflux assay. Negative control and *MtMATE67*-expressing oocytes were injected with [^{14}C]-labeled citrate or ferric citrate, and the efflux of radiolabel was assayed after 2-h incubation in Ringer's solution pH 5.5. Error bars represent SE, $n = 2$ to 3 ($n = 2$; Fe-citrate control). **Two-way ANOVA test with correction for multiple comparisons, P value < 0.01. C, Current-voltage plots from two-electrode voltage clamp recordings of *MtMATE67*-expressing oocytes injected with citrate or Fe-citrate as in B. Steady-state currents at the indicated clamped potentials were measured 30 min after substrate injection. Recordings were done in Ringers solution buffered either at pH 5.5 or 7.5. D, Comparison of steady-state inward currents generated by citric acid- or Fe-citrate-injected oocytes at −80 mV. The currents were background corrected by subtraction of currents measured with negative control oocytes. Error bars represent SE ($n = 2$–4; $n = 2$: pH 7.5 data; $n = 4$: pH 5.5 data). ***Two-way ANOVA test with correction for multiple comparisons, P value < 0.001. The data shown in this figure are representative results consistent with multiple assays using other oocyte batches.

nodule primordium (Fig. 2C). At 4 dpi, GUS staining was observed in the nodule primordium (Fig. 2D). In 10 dpi nodules, GUS expression was associated with the invasion zone, but not with the nitrogen-fixation zone (Fig. 2, E and G, whole nodule; Fig. 2F, longitudinal section). In mature, 38 dpi nodules, GUS staining was observed primarily in the distal invasion zone and vascular bundles (Fig. 2, H and I). The activity pattern generated with the R108-derived promoter in mature nodules (Supplemental Fig. S3) was essentially the same as observed with the corresponding promoter from genotype A17 (Fig. 2, H and I). Together, our qRT-PCR and GUS staining data indicated early induction of *MtMATE67* expression in the nodule primordium and cortical cells of nascent nodules and prominent expression in the invasion zone of mature nodules.

MtMATE67 Is an Fe-Activated Citrate Transporter

Phylogenetic analysis showed that MtMATE67 segregates into a clade that includes the citrate efflux transporters LjMATE1 and AtFRD3 (Fig. 1). To investigate whether MtMATE67 shares this activity or whether it possesses other transport functions, its activity was characterized by heterologous expression and transport analyses in the *Xenopus laevis* oocyte expression system. Based on lack of success with native cDNAs, a codon-optimized synthetic gene was developed which resulted in strong expression by using *X. laevis* oocytes (Fig. 3A). Oocytes expressing MtMATE67 showed no significant differences to negative-control oocytes in either uptake or efflux activity for radiolabeled citrate (Fig. 3B; Supplemental Fig. S4). However, upon injection of [^{14}C]-labeled ferric citrate, MtMATE67 oocytes showed a substantial increase (5-fold over control oocytes) in the efflux of radiolabel (Fig. 3B). Similar to other MATE activities (Moriyama et al., 2008; Takanashi et al., 2014), this activity was specific for efflux, and there was no difference in the uptake of [^{14}C]-labeled citrate supplied as an Fe(III)-chelate between MtMATE67 and control oocytes (Supplemental Fig. S4). These observations were supported by two-electrode voltage clamp recordings that showed a high inward current for MtMATE67 oocytes injected with Fe-citrate (Fig. 3, C and D). By convention, inward

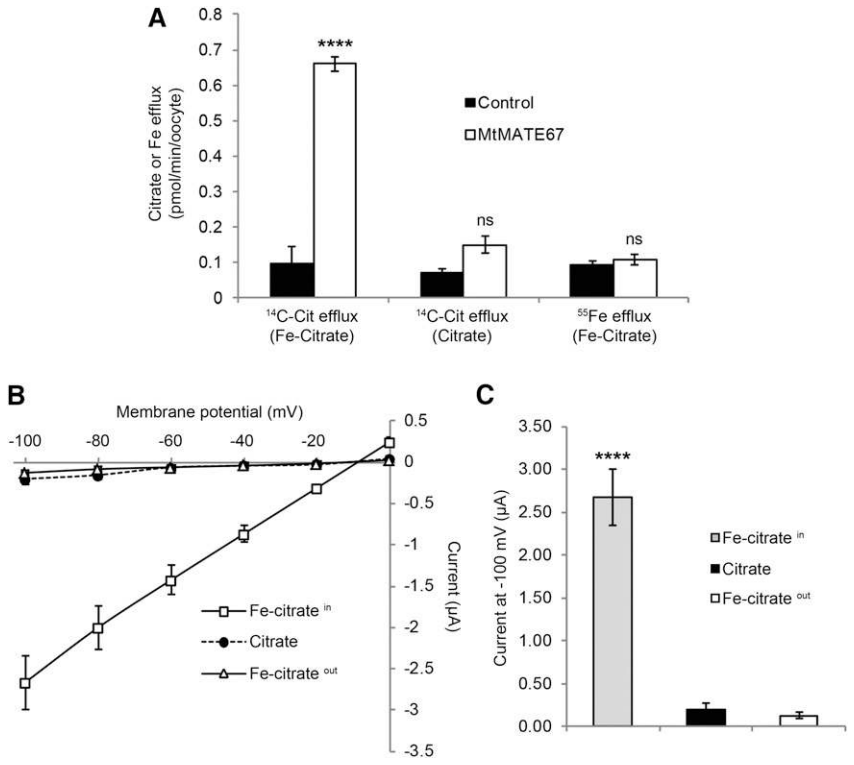

Figure 4. MtMATE67 transports citrate but not Fe and is activated by Fe on the cytosolic side. A, Efflux of radiolabeled substrates from *X. laevis* oocytes microinjected with [^{14}C]-Fe-citrate, [^{14}C]-citrate, or with [^{55}Fe]-citrate. The rate of efflux was assayed over a 2-h period. Cross-hatched bars represent *MtMATE67*-expressing oocytes and solid bars are negative control oocytes. Error bars represent SE (n = 3–4). ****Two-way ANOVA test with correction for multiple comparisons, P value < 0.0001. B, Current-voltage plots of *MtMATE67*-expressing oocytes. Citrate, oocytes injected with 2.5 mM citrate; Fe-citrate^{out}, oocytes injected with 2.5 mM citrate, with 2 mM Fe-citrate in the bath; Fe-citrate^{in}, oocytes injected with 2.5 mM Fe-citrate. All recordings were done in modified Ringer's solution, pH 5.5. Data were background corrected by subtraction of currents obtained with control oocytes. C, The mean steady-state inward currents at −100 mV. The error bars represent SE (n = 5–6). ****One-way ANOVA test with correction for multiple comparisons, P value < 0.0001.

currents indicate the influx of net positive charge or the efflux of net negative charge (see, for example Durrett et al., 2007). Transport through MATEs is driven by the antiport cotransport of either a proton or cation (Lu, 2016). Consistent with this, the inward current shown in Fe-citrate-injected MtMATE67 oocytes is dependent on a pH gradient, and recordings in neutral pH Ringers solution resulted in the loss of inward current (Fig. 3, C and D).

Further analysis showed that the robust MtMATE67 currents depended on injection of Fe-citrate. Injection with other citrate salts (Supplemental Fig. S5), including Al-citrate, which induces the activity of other MATEs (Furukawa et al., 2007), resulted in lower currents compared to Fe-citrate. Interestingly, ferric chloride showed an increase in current, although it was much less than what was observed for ferric citrate. These results indicated that both Fe and citrate injection are required for MtMATE67 transport. Two other organic acids, namely malic acid and succinic acid, are unlikely to be substrates for MtMATE67 efflux activity, as indicated by very low currents that were similar to those associated with citric acid in the absence of Fe (Supplemental Fig. S6).

To investigate whether MtMATE67 cotransports Fe and citrate, efflux assays were performed with MtMATE67 oocytes injected with [^{14}C]-labeled Fe-citrate, [^{55}Fe]-labeled Fe-citrate, or [^{14}C]-citrate. Injection of [^{55}Fe]-labeled Fe-citrate showed no additional efflux of radiolabeled Fe compared to control oocytes (Fig. 4A). In contrast, MtMATE67 significantly increased [^{14}C]-citrate efflux from Fe-citrate-loaded oocytes but not those loaded with citrate alone (Fig. 4A). The data suggest that although MtMATE67 requires Fe-citrate for its activity, it transports only citrate and not Fe. It is proposed that Fe, perhaps in a complex with citrate, activates the citrate transport efflux activity of MtMATE67. To determine whether the stimulatory effect of Fe-citrate is exerted on the extracellular or intracellular side of the transporter, voltage clamp recordings were done with Fe-citrate injection or by placing Fe-citrate in the recording bath (Fig. 4, B and C). Voltage clamp recordings show that MtMATE67 currents were only induced when Fe-citrate was injected into the oocyte along with citrate (Fe-citrate^{in}), but not when oocytes were injected with citrate alone with 2 mM Fe-citrate supplemented in the external bath solution (Fe-citrate^{out}; Fig. 4, B and C). Taken together, the results indicate that MtMATE67 is a citrate efflux transporter that is stimulated by the presence of Fe inside the cell.

Localization of MtMATE67 to the PM of Infected and Uninfected Cells

To visualize the subcellular location of MtMATE67, we generated a C-terminal MtMATE67-hemagglutinin (HA)-tag fusion construct, using genomic DNA of *MtMATE67* that included 2,037 bp of its native promoter. This construct was expressed in transgenic roots following transformation with *Agrobacterium rhizogenes* (Fig. 5). The HA-tag on the MtMATE67-HA fusion protein was visualized using an anti-HA mouse monoclonal antibody and an anti-mouse rabbit monoclonal

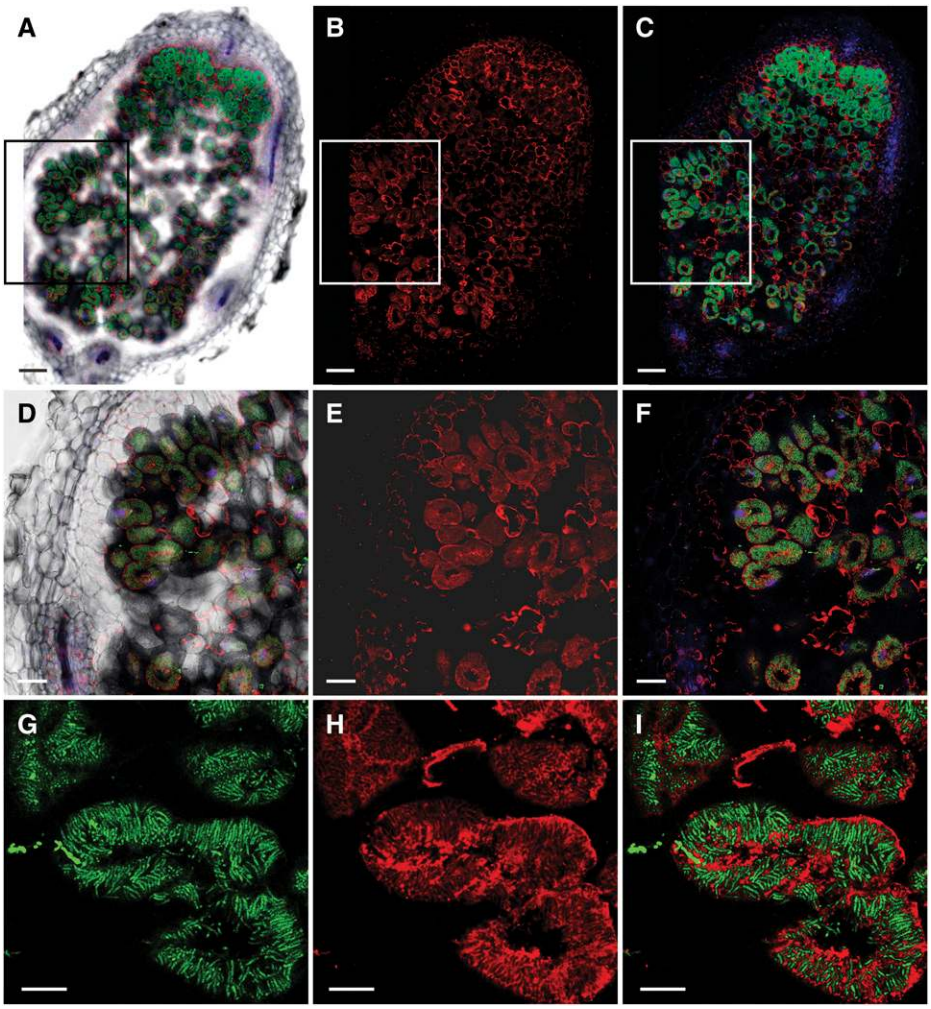

Figure 5. Subcellular localization of MtMATE67-HA fusion driven by the native promoter and visualized with an anti-HA antibody. Images were acquired with a confocal laser scanning microscope. Rhizobia in these images express GFP. The anti-HA antibody is coupled with the Alexa 594 fluorescent dye. A to C, Whole-nodule image (28 dpi). D to F, Zoom-in regions that correspond to rectangles in A to C. G to I, Close-up of an infected nodule cell. Red channel: anti-HA antibody. Green channel: GFP-expressing rhizobia. A and D, Overlay images of bright-field, red, and green channels. C, F, and I, Overlay images of red and green channels. Anti-HA antibody colocalizes with the PMs of infected, noninfected, and cortical cells throughout the nodule (A–F). The tag also localizes to the periphery of bacteroids, presumably the SM (H and I). Bars = 100 μm in A to C, 50 μm in D to F, and 20 μm in G to I.

antibody coupled to the red-fluorescent dye, Alexa 594. Nodules were induced on transgenic roots using a GFP-expressing strain of *Sinorhizobium meliloti*. Red fluorescence associated with MtMATE67-HA-expressing nodules was found mainly in nodule zones II and III, and was localized on the periphery of infected and uninfected cells, consistent with localization to the PM (Fig. 5, A–C). Red fluorescent signal was also detected inside infected nodule cells, separate from the cell periphery (Fig. 5, D–I). No red background fluorescence signal was detected in untransformed negative control nodules stained in the same way as the HA-expressing nodules (Supplemental Fig. S7). In another experiment, expression of an MtMATE67-GFP fusion protein in transgenic nodules, driven by the constitutive maize (*Zea mays*) polyubiquitin promoter, resulted in green fluorescence on the PM of uninfected cells and on internal membranes of infected, bacteroid-containing cells (Supplemental Fig. S8, A–D). Greater magnification revealed that green fluorescence coincided with the red fluorescence emitted by RFP-expressing bacteria from infected cells (Supplemental Fig. S8, E and F), indicating that MtMATE67 may be located in the SM surrounding bacteroids.

mate67 Mutants Are Impaired in SNF, Plant Growth, and Fe Distribution

To elucidate the physiological role of *MtMATE67*, we isolated two retrotransposon *Tnt1* insertional mutant lines, NF3177 (*mate67-1*) and NF11278 (*mate67-2*), bearing *Tnt1* insertions in exon 3 and 4 of *MtMATE67*, respectively (Supplemental Fig. S9). In contrast to wild-type nodules, nodules of the two mutants failed to develop the pink color characteristic of leghemoglobin, by 8 dpi (Supplemental Fig. S10). Additionally, nodules of *mate67* mutants were smaller than those of the wild-type from 10 dpi onwards (Supplemental Fig. S10). Nitrogen-fixation activity of the *mate67* mutants was measured using the acetylene reduction assay, which revealed an approximately 4-fold decrease in nitrogenase activity in the two mutants compared to the wild-type at 15 dpi (Fig. 6). Consistent with this, *mate67* mutant plants were significantly smaller than wild-type

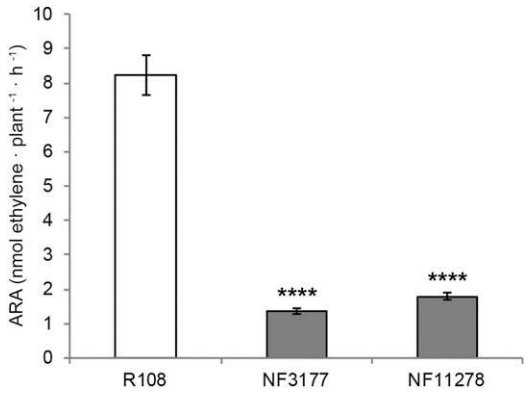

Figure 6. Nitrogenase acetylene reduction activity (ARA) measured 15 dpi in wild-type (R108) and two mutant lines of *MtMATE67* (NF3177 and NF11278). Error bars indicate SE ($n = 34–37$). ****One-way ANOVA test with correction for multiple comparisons, P value < 0.0001, comparison with R108.

plants when reliant on SNF for growth (Fig. 7). On the other hand, provision of mineral nitrogen to *mate67* mutants restored growth to wild-type levels, consistent with a symbiosis-specific role of MtMATE67 in plant nitrogen nutrition (Fig. 7). Genotyping of backcross 2 (BC2) populations segregating for the fix phenotype indicated 100% linkage to the homozygous state of *Tnt1* insertion in *MtMATE67* (Supplemental Table S2).

To confirm that *Tnt1* insertions in *MtMATE67* were responsible for the symbiotic mutant phenotype, we conducted genetic complementation of *mate67* mutants, using the wild-type *MtMATE67* coding sequence (CDS) and promoter. DsRed was used as a reporter to identify transformed roots and nodules. *A. rhizogenes*-mediated transformation of homozygous *mate67* plants from both lines, NF3177 and NF11278, and subsequent inoculation with *S. meliloti* resulted in pink wild-type-like nodules with increased nitrogenase activity compared to noncomplemented mutant controls, while only white nodules were observed on untransformed roots of the complemented plants (Supplemental Fig. S11).

Transmission electron microscopy (TEM) was used to assess the morphology and fate of bacteroids in *mate67* nodules. TEM revealed that bacteroids at the distal end of the nitrogen-fixation zone in *mate67* nodules were elongated, with electron-dense and electron-translucent regions, as in wild-type plants (Supplemental Fig. S12, A and B). On the other hand, bacteroids were irregularly shaped in plant cells at the root-proximal end of 10 dpi mutant nodules, and these plant cells contained multiple vacuoles, in contrast to those of the wild type (Supplemental Fig. S12C). Additionally, nuclei of *mate67*-, but not wild-type, infected cells contained electron-dense bodies other than nucleoli in the nitrogen-fixation zone (Supplemental Fig. S12, B and C). Light microscopy on sections of 21 dpi *mate67* nodules revealed

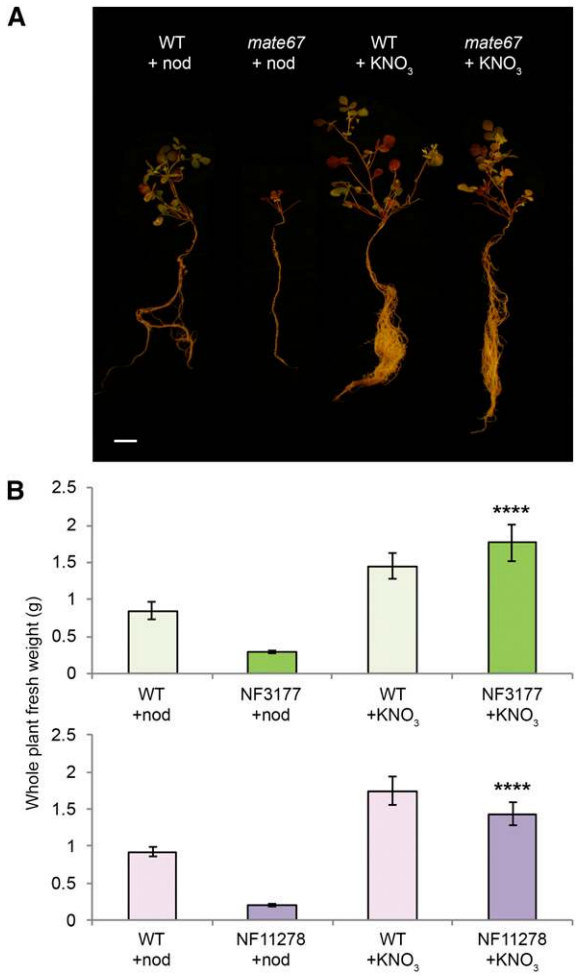

Figure 7. Complementation of *mate67* mutants with nitrate. A, Plants representing mutant line NF11278 and corresponding wild-type-like siblings (WT). Left-hand side: plants grown with rhizobia (+nod). Right-hand side: plants grown with 2 M KNO_3 (+KNO_3). Bar = 1 cm. B, Whole-plant fresh weight of the mutant and wild-type-like plants. Error bars indicate SE ($n = 7–12$). ****Two-way ANOVA test with correction for multiple comparisons, P value < 0.0001, comparison with NF3177+nod and NF11278+nod, respectively. Note that there was no significant difference between KNO_3-treated wild-type and mutant plants, indicative of full rescue of the mutant phenotype by addition of nitrogen.

relatively few *lacZ*-expressing rhizobia, compared to the wild-type, as judged by X-Gal staining (Supplemental Fig. S13), while brown material, presumably phenolic compounds (Bourcy et al., 2013; Sinharoy et al., 2013), was evident in mutant but not wild-type nodules.

In view of the citrate efflux activity of MtMATE67 (Fig. 3), we were keen to compare the distribution of Fe in *mate67* and wild-type nodules. Synchrotron x-ray fluorescence (SXRF) microspectrometry revealed an accumulation of Fe around infected cells (apparently in the apoplasm) in the nitrogen-fixation zone of mutant but not wild-type nodules (Fig. 8).

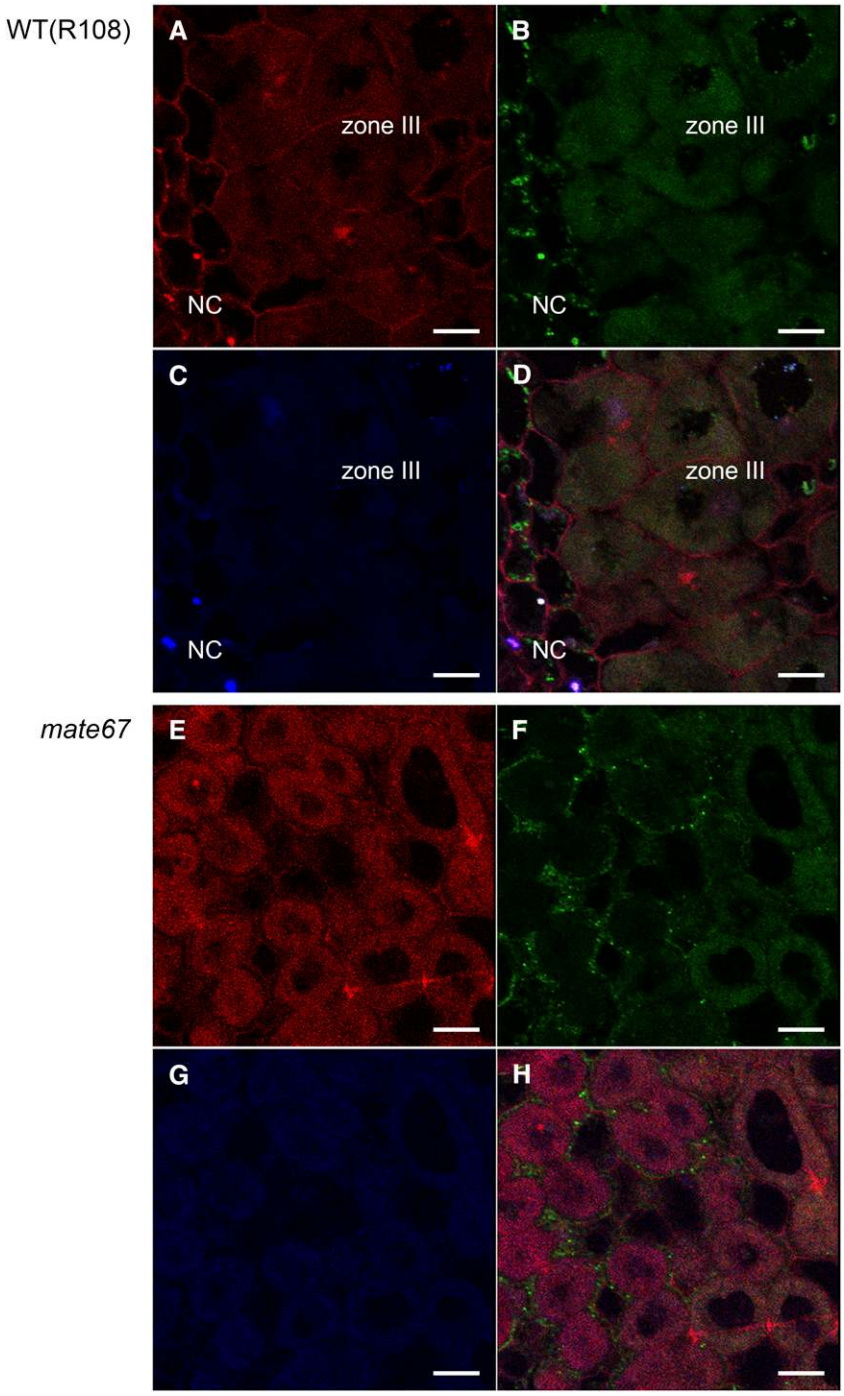

Figure 8. SXRF microspectrometry imaging of Fe nuclei, along with Ca and Zn, in nodules (12 dpi) of wild-type R108 (A–D) and *mate67* line NF3177 (E–H). Images in A to D represent a border region between the nodule cortex (NC) and colonized cells from the nitrogen-fixation zone (zone III). Images in E to H represent the nitrogen-fixation zone. Green color indicates Fe, while images showing Ca (red) and Zn (blue) distribution were added to outline cell walls and the plasma membranes, respectively. Bars = 20 μm. Note accumulation of Fe around infected cells of the mutant (apparently apoplasm).

DISCUSSION

We have shown here that MtMATE67 is an Fe-activated citrate transporter required for Fe homeostasis that is specialized for symbiosis and essential for SNF in *M. truncatula*. Novel findings presented here include Fe activation of a MATE transporter and localization of a MATE protein to two different membrane systems, indicating distinct physiological roles in different cell types.

Similar to other MATE family members (Lu, 2016), topology and modeling analyses of MtMATE67 show the typical MATE fold consisting of 12 predicted α-helices divided into 2 symmetry-related clusters of 6 α-helices that likely form the transport pore (Supplemental Fig. S2). Phylogenetic analysis of MtMATE67 placed it into a clade of 25 proteins, most of which are documented citrate transporters (Takanashi et al., 2014; Supplemental Table S1, and references therein). Members of this clade are distinguished by the

presence of an extended predicted intracellular loop (62–116 amino acid residues in length) between transmembrane domains 2 and 3 (Supplemental Fig. S14; Liu et al., 2009; Meyer et al., 2010). The structural and functional significance of this loop is not yet known. Members of the citrate transporting clade of MATEs have been proposed to play a role in citrate efflux to chelate and mobilize Fe^{3+} in the apoplasm or xylem (e.g. Arabidopsis FRD3; Durrett et al., 2007) or as aluminum-activated citrate efflux channels that ameliorate the toxic effects accompanying Al^{3+} accumulation in acidic soils (for review, see Kochian et al., 2015; Shoji, 2014).

Evidence that MtMATE67 forms a citrate efflux channel that is essential for Fe homeostasis in nodules comes from the following observations. Similar to other eukaryotic MATE proteins, which are secondary transporters coupled to H^+ gradients (Lu, 2016), MtMATE67 shows a pH-dependent citrate efflux activity in *X. laevis* oocytes, based on radiolabeled substrate and two-electrode voltage clamp analyses (Fig. 3). *Tnt1* mutants of MtMATE67 show a fix phenotype with SXRF microspectrometry indicating the accumulation of Fe deposits within the apoplasm between infected cells of zone III (Fig. 8). This latter observation is reminiscent of the phenotype observed with Arabidopsis FRD3, a citrate efflux transporter that provides citrate for Fe-citrate transport within the xylem for distribution to tissues throughout the plant (Green and Rogers, 2004; Durrett et al., 2007). Fe delivery to the developing nodule is thought to occur through Fe-citrate from xylem vessels (Brear et al., 2013). Two pathways (symplasmic and apoplasmic) are proposed for subsequent delivery of Fe to sites of need (Brear et al., 2013). Based on its activity and localization within the distal nitrogen-fixation zone and infected zones, MtMATE67 may play multiple roles in regulating ferric citrate solubility and mobility within the apoplasm, a role consistent with the observation that *mate67* mutants have abnormal apoplasmic Fe deposits (presumably insoluble ferric Fe).

In addition to the PM localization, MtMATE67 appeared to be localized to symbiosomes (Supplemental Fig. S8), most likely the SM. The symbiosome space between the SM and bacteroids contains Fe chelated to siderophores, in some cases citrate (LeVier et al., 1996; Brear et al., 2013). Thus, an additional function for the citrate transport activity of MtMATE67 could be to mediate the flux of citrate from the infected cell cytosol to the symbiosome space.

A novel feature of MtMATE67, not observed previously with other citrate-transporting MATEs, is the activation of citrate efflux by Fe(III). Previous work with MATEs in the FRD3 subfamily has demonstrated the activation of citrate efflux by Al^{3+} (Furukawa et al., 2007). Analysis of MtMATE67 showed that Fe(III)-citrate, but not Al-citrate activated citrate efflux, indicating that MtMATE67 may be distinct from other members of the FRD3 subfamily in its mode of action (Supplemental Fig. S5). Fe activation of citrate transport across the SM may help to coordinate citrate efflux with Fe efflux via a separate transporter for transient storage of Fe-citrate in the symbiosome space, prior to Fe uptake by bacteroids. Regulation by Fe would avoid unnecessary and potentially wasteful efflux of citrate when it is not needed.

Support for Fe-activated citrate transport across the SM comes from previous biochemical analyses of isolated soybean symbiosomes (Moreau et al., 1995). By using radiolabeled substrates, it was shown that soybean symbiosomes require Fe(III) for citrate uptake (Moreau et al., 1995). If this feature is conserved between *M. truncatula* and soybean, the activation of citrate efflux by Fe(III) observed for MtMATE67 provides a mechanism that explains the biochemical data of Moreau et al. (1995).

While the benefit of Fe activation of citrate efflux by MtMATE67 at the SM seems clear, it is less clear what purpose this would serve at the PM. One hypothesis is that citrate efflux to the apoplasm under conditions of Fe sufficiency could help to lock Fe in a benign form in the apoplasm until Fe is once again required by the cell, partly analogous to how Al-activated MATE transporters release citrate to complex Al and keep it out of root cells (Yokosho et al., 2011). Whether citrate released from the cell by MtMATE67 serves to sequester Fe in the apoplasm or helps to make it available for uptake by the cell presumably depends on the activities of ferric-chelate reductase oxidase and/or Fe transporters on the PM, which are regulated by Fe availability/demand (for review, see Kobayashi and Nishizawa, 2012).

During our investigation of the substrate selectivity of MtMATE67, we also examined whether the transporter is able to flux the structurally related substrate homocitrate. Homocitrate is an essential cofactor of the Fe-molybdenum component of nitrogenase (Hoover et al., 1989), which needs to be supplied by the host to nitrogen-fixing bacteroids, at least in some symbioses (Hakoyama et al., 2009; Terpolilli et al., 2012). Oocytes expressing MtMATE67 showed a low but significant current induced by injection of homocitrate (Supplemental Fig. S5), which was similar to that produced by the injection of citrate alone. While this activity is much lower than the Fe-induced citrate currents, given its potential localization on the SM, an additional function for MtMATE67 could be to assist in the uptake of homocitrate into the symbiosome.

Nodule-induced expression of the *MtMATE67* gene (Fig. 2; Supplemental Fig. S1) and the symbiosis-specific fix phenotype of the *mate67* mutant (Fig. 7) indicate that this gene is specialized for its role in symbiosis. Likewise, nodule-specific expression of *LjMATE1*, which is in the same subclade as *MtMATE67* (Fig. 1), indicates that it is also specialized and required for SNF. Indeed, this appears to be the case based on partial loss-of-function of *LjMATE1* resulting from RNA interference (Takanashi et al., 2013). Like the *mate67* mutant of *M. truncatula*, an *LjMATE1* RNAi line of *L. japonicus* exhibited aberrant Fe homeostasis, with Fe accumulating in nodule vascular tissues and

declining in the infected zone (Takanashi et al., 2013). This contrasts somewhat with our results that show accumulation of Fe in the apoplasm of nodule cells in the nitrogen-fixation zone on the *mate67* mutant (Fig. 8), which may reflect differences between indeterminate (*M. truncatula*) and determinate (*L. japonicus*) nodules.

Despite premature senescence of rhizobia in *mate67* nodules (Supplemental Fig. S12), residual nitrogenase activity indicated that some rhizobia differentiate fully into bacteroids in these mutant nodules (Fig. 6). Consistent with this, we observed what appeared to be fully mature bacteroids by TEM of 10 dpi nodule sections (Supplemental Fig. S12; c.f. Vasse et al., 1990). Interestingly, numerous small vacuoles in infected nodule cells of *mate67* mutant plants were observed (Supplemental Fig. S12C), resembling the *sen1* mutant phenotype of *L. japonicus* (Hakoyama et al., 2012). SEN1 belongs to the family of VIT and is thought to deliver Fe to symbiosomes. Like *mate67*, *sen1* mutants are defective in SNF (Hakoyama et al., 2012; Suganuma et al., 2003).

Our results point to symbiotic roles for MtMATE67 in the supply of Fe to cells of developing as well as mature, nitrogen-fixing nodules. Relatively high expression of *MtMATE67* in the nodule invasion and distal nitrogen-fixation zones points to an important role for Fe supply to these cells. Consistent with this, plant and bacterial genes encoding Fe-containing proteins, including plant leghemoglobins and bacterial nitrogenase components, are coexpressed with MtMATE67 in nodules (Benedito et al., 2008; Roux et al., 2014; Supplemental Tables S3 and S4).

The data presented here support and extend a proposed model of Fe delivery to rhizobia-containing cells (Tejada-Jiménez et al., 2015) in which citrate is required in the apoplasm of nodule cells to ensure solubility and mobility of Fe before MtNramp1 translocates Fe across the PM. Once in the cytosol, Fe may be transported across the SM by MtSEN1 in a process supported by citrate chelation of-Fe in the symbiosome space. Citrate transport out of the cytoplasm across both the PM and SM is proposed to involve one or more MATE transporters (Tejada-Jiménez et al., 2015). Our results indicate that MtMATE67 plays a role in both of these processes that are crucial to the supply of Fe to plant and bacterial cells of legume root nodules.

MATERIALS AND METHODS

Gene Identification and Phylogenetic Analysis

MtMATE67 was identified due to its nodule-specific expression profile (probeset Mtr.3624.1.S1_at), using the MtGEA Web server available at http://mtgea.noble.org/v3/ (Benedito et al., 2008; He et al., 2009). Alignment of the deduced amino acid sequences of MtMATE67 and 69 published plant proteins of the MATE family (Fig. 1; Supplemental Data Set S3; Supplemental Table S1) was performed using multiple sequence comparison in the MEGA v7.0.21 software suite (Kumar et al., 2016). A phylogenetic tree was built using the maximum parsimony method with arithmetic mean of 1,000 bootstrap replicates. The protein sequences were manually trimmed from the N terminus and C terminus to a consensus sequence before the alignment.

Insertional Mutant Screening, Genotyping, and Backcrossing

Generation of the *Medicago truncatula Tnt1* insertional mutant population and growth of R1 generation seeds were described previously (Tadege et al., 2008). Reverse genetic screening for *Tnt1* retrotransposon insertions in *MtMATE67* was performed using a nested PCR approach (Cheng et al., 2011). All primer sequences used in this study are given in Supplemental Table S5. Homozygous mutant plants were isolated from R2 generation seeds using primers described in Supplemental Table S5. Back-crossing of mutants to the wild-type R108 was performed as described (Taylor et al., 2011; Veerappan et al., 2014). Genotyping was conducted on segregating BC2 populations (i.e. the offspring of a self-pollinated heterozygous mutant isolated after two consecutive backcrosses to the wild-type R108).

Nodulation Assays and Sample Collection

M. truncatula ecotype R108 and homozygous *mate67* mutants of lines NF3177 (*mate67-1*) and NF11278 (*mate67-2*) were used for nodulation assays. Seeds were scarified for 8 min in concentrated H_2SO_4, rinsed five times with sterile cold water followed by sterilization for 3 min with 30% (v/v) commercial bleach containing a few drops of Tween 20, and washed 10 times with sterile water. Seedlings were transferred to cone-shaped pots containing a mixture of turface and vermiculite (2:1). Plants were grown under a 16-h-light/8-h-dark regime, 200 μE m^{-2} s^{-1} light intensity, 21°C day/night and 40% relative humidity. Seven days after transplanting, plants were inoculated with 50 mL suspension of *Sinorhizobium meliloti* strains 1021, 1021 with pXLGD4 plasmid containing *lacZ* reporter gene (Boivin et al., 1990), 1021 with a GFP-expressing plasmid pHC60 (Cheng and Walker, 1998), or 1021 with a plasmid pQDN03 expressing mCherry (Haney and Long, 2010). *S. meliloti* strains were grown overnight in TY liquid medium up to OD_{600} ~1.0, pelleted by centrifugation, and resuspended in half-strength B&D (Broughton and Dilworth, 1971) with 0.5 mM KNO_3 to an OD_{600} ~0.02. For nodulation time course assays, susceptible root zones were harvested for 0 to 4 dpi samples. From 6 dpi onwards, only portions of the roots carrying clearly visible nodules were excised and immediately frozen in liquid nitrogen. To measure *MtMATE67* expression by qRT-PCR in different nodule zones, 28 dpi wild-type nodules (Jemalong A17) were manually dissected into the meristematic zone, invasion zone, distal nitrogen-fixation zone, nitrogen-fixation zone, and senescence zone, as described previously (Sinharoy et al., 2013; Guefrachi et al., 2014).

RNA Extraction, qRT-PCR, and Microarray Analyses

Total RNA was extracted using TRIzol reagent (Life Technologies), followed by genomic DNA removal with DNase 1 (Ambion) and additional column purification with an RNeasy MinElute CleanUp Kit (Qiagen). RNA was quantified using a Nanodrop Spectrophotometer ND-100 (NanoDrop Technologies) and the purity assessed with a Bioanalyzer 2100 (Agilent). For qRT-PCR, RT was carried out using SuperScript III Reverse Transcriptase (Invitrogen) and oligo$(dT)_{20}$ to prime the reaction, as describe previously (Kakar et al., 2008). Transcript levels were normalized using the geometric mean of three housekeeping genes, *MtPI4K* (*Medtr3g091400*), *MtPTB2* (*Medtr3g090960*), and *MtUBC28* (*Medtr7g116940*), whose transcript levels were stable across all the samples analyzed. Three biological replicates were included per gene and displayed as relative expression values. qRT-PCR and microarray hybridization protocols were as described previously (Kryvoruchko et al., 2016). Primer sequences used in this analysis are given in Supplemental Table S5.

Generation of Constructs for *MtMATE67* Promoter Activity, Protein Localization, and Genetic Complementation

A construct for MtMATE67 immunolocalization experiments was prepared by cloning genomic DNA of *MtMATE67* (ecotype R108), including 2,037 bp of its promoter, into vector pGWB13 (Nakagawa et al., 2007). For promoter-GUS activity analysis, *MtMATE67* promoter sequence (2,928 bp) immediately upstream of the start codon was amplified from gDNA of ecotype A17, and subsequently introduced into vector pKGWFS7,0 (Karimi et al., 2002) for fusion with the GUS reporter gene. *MtMATE67* coding region was cloned from cDNA of 21 dpi nodules (R108). For constitutive expression using the maize (*Zea mays*) polyubiquitin promoter, the CDS was introduced into vector pUBIcGFP

(Kryvoruchko et al., 2016) that combined the backbone of pMBb7Fm21GW-UBIL (VIB, Flemish Institute for Biotechnology) with the DsRed cassette from pKGW RedRoot (VIB). For protein localization using the native promoter, a fusion construct joining 2,928 bp of promoter (ecotype A17) and the CDS (ecotype R108) was prepared by overlap PCR, as described by Kryvoruchko et al. (2016) (primer sequences for all cloning steps are given in Supplemental Table S5). The resulting construct was introduced into vector pRRcGFP (Kryvoruchko et al., 2016), in which the backbone of pKGW RedRoot (VIB) was supplemented with eGFP (plus terminator) from pK7FWG2 (Karimi et al., 2002). This native promoter-CDS fusion was also used for the genetic complementation of *mate67* mutants. The constructs were introduced into *Agrobacterium rhizogenes* strain ARqua1 (Quandt et al., 1993) for infection of the mutant and R108 seedlings to generate composite plants (Boisson-Dernier et al., 2001). Transformed hairy roots were screened for the DsRed signal under a fluorescent stereo microscope (protein localization, complementation) or used directly for GUS staining. Roots transformed with the empty vectors and nontransformed roots from the same plants were used as controls.

Transport Assays and Electrophysiology of MtMATE67 in *Xenopus laevis* oocytes

Expression of *MtMATE67* in *X. laevis* oocytes was done by the general approach of Vincill et al. (2005). Early experiments with *MtMATE67* cDNA resulted in low expression of this gene in oocytes. Thus, a codon-optimized synthetic version of *MtMATE67* (optiMATE) was designed using the strategy of Feng et al. (2013) and synthesized by GenScript (see Supplemental Data Set S1 for the sequence). The optiMATE gene was cloned into the *Bgl*II and *Spe*I restriction sites of the pT7TS *X. laevis* expression vector downstream of T7 promoter with in-frame C-terminal FLAG tag separated from the *MtMATE67* ORF with a Gly-Gly-Gly linker (Krieg and Melton, 1984). OptiMATE cRNA was synthesized by in vitro transcription using mMESSAGE mMACHINE kit (Life Technologies), as previously described (Vincill et al., 2005). *X. laevis* oocytes (stage VI) were surgically harvested, defolliculated, and microinjected with 46 nL of cRNA, or an equivalent volume of sterile water (negative control), and subsequently incubated in Ringer's solution (96 mM NaCl, 2 mM KCl, 5 mM $MgCl_2$, 0.6 mM $CaCl_2$, and 5 mM HEPES-NaOH, pH 7.6) supplemented with 1000 units of penicillin-streptomycin (Sigma-Aldrich) for 2 d at 16°C prior to analysis.

Activity analyses were conducted using uptake or efflux of a radiolabeled substrate, or the two-electrode voltage clamp method. For uptake assays, oocytes (three oocytes/replicate) were incubated in 250 μL of Frog Ringer's solution supplemented with 100 μM of 0.1 nCi/μL [^{14}C]-labeled citric acid (Moravek Biochemicals) or 100 μM of 0.1 nCi/μL [^{14}C]-labeled ferric citrate for 30 min at room temperature. Oocytes were washed three times with 500 μL of Ringer's solution in each wash, and uptake was determined by lysing the oocytes in 200 μL of 10% (w/v) SDS, followed by liquid scintillation counting with a Beckman Coulter LSC.

For [^{14}C]-citrate efflux assays, oocytes were injected with 46 nL of 0.05 μCi/μL [^{14}C]-labeled 2.5 mM citrate or 0.05 μCi/μL [^{14}C]-labeled 2.5 mM Fe-citrate (Furukawa et al., 2007). The oocytes were placed in modified Ringer's solution, pH 5.5, and the efflux of radiolabel was assayed at 16°C for 2 h by scintillation counting. The radioactivity of the efflux solution and homogenized oocytes were measured separately, and the ratio was calculated by dividing the radioactivity of the efflux solution by the total oocyte radioactivity.

To investigate the cotransport of citrate and Fe by MtMATE67, the efflux assay was repeated with [^{55}Fe]-labeled Fe-citrate and compared to the efflux of [^{14}C]-labeled 2.5 mM Fe-citrate. [^{55}Fe]-labeled Fe-citrate was prepared by mixing 2 μCi/μL of [^{55}Fe]-labeled $FeCl_3$ (Perkin-Elmer) with citric acid at a 1:100 molar ratio (which favors the formation of the mononuclear Fe-citrate species [Silva et al., 2009]) at room temperature for 1 d prior to the experiment. Oocytes were injected with 46 nL of either 0.06 μCi/μL [^{14}C]-labeled citrate/Fe-citrate or 1 μCi/μL of [^{55}Fe]-labeled Fe-citrate. Oocytes were placed in modified Ringer's solution (pH 5.5) at 23°C, and the rate of [^{14}C] or [^{55}Fe] release from the oocytes into the bath solution was assayed.

The electrophysiological analysis of the oocytes was performed by the two-electrode voltage clamp recording using Oocyte Clamp Amplifier model OC-725C (Warner Instruments), as described by Vincill et al. (2005). Steady-state currents were recorded at membrane voltage potentials in 20-mV steps over a range of −100 to 0 mV. Each potential was maintained for 1 s and followed by a 0.5-s recovery period between voltage pulses. The oocytes were injected with 2.5 mM of the test substrates 30 min prior to the voltage clamp analysis. To compare the effects of Fe-citrate inside and outside of the oocyte, recordings were done in oocytes injected with either Fe-citrate (Fe-citrate^{in}) or citrate (Fe-citrate^{out}), and the currents were recorded by placing the oocytes in modified Ringer's solution (pH 5.5) with (Fe-citrate^{out}) or without (Fe-citrate^{in}) 2 mM Fe-citrate.

Immunolocalization of MtMATE67

Analysis of MtMATE67 localization using an HA-tag-based approach was conducted as described by Tejada-Jiménez et al. (2015). Nodules collected from 28-dpi plants were fixed by overnight incubation in 4% paraformaldehyde, 2.5% Suc in PBS at 4°C. After washing in PBS, nodules were cut in 100-μm sections with a Vibratome 1000 plus (Vibratome). Sections were dehydrated in methanol series (30, 50, 70, and 100% in PBS) for 5 min at each step and then rehydrated in methanol/PBS concentration series in reverse order. Cell walls were treated with 4% cellulase in PBS for 1 h at room temperature and with 0.1% Tween 20 in PBS for additional 15 min. Sections on immunology slides were blocked with 5% bovine serum albumin in PBS before incubating them with an anti-HA mouse monoclonal antibody (Sigma-Aldrich) for 2 h at room temperature. After washing, an Alexa 594-conjugated anti-mouse rabbit monoclonal antibody (Sigma-Aldrich) was added to the sections and incubated for 1 h at room temperature. DNA was stained with DAPI after washing. Images were acquired with a confocal laser scanning microscope Leica SP8 (Leica Microsystems).

Phenotypic Analysis, Histochemical Staining, Confocal Electron Microscopy, and TEM

Images of whole-mount nodulated roots were captured using an Olympus SZX12 stereomicroscope (Olympus) equipped with a Nikon DXM1200C digital camera (Nikon Instruments). Histochemical staining with X-Gal was performed as described previously (Boivin et al., 1990). The dual staining for GUS and rhizobia (Magenta-Gal) was conducted as described by Pislariu and Dickstein (2007). Detached nodules were embedded in 5% low melting point agarose and sliced into 50-μm-thick sections with a Vibratome 1000 Plus (Vibratome). For confocal microscopy with the GFP tag, sample preparation was done according to Haynes et al. (2004). Nodules were sliced manually and stained with SYTO13 and/or calcofluor (Life Technologies). For image acquisition, we used a Leica TCS SP2 AOBS confocal laser scanning microscope and LCS Lite 2.0 software (Leica Microsystems) or a Perkin-Elmer Ultra View Spinning Disc confocal microscope supplied with Velocity 6.1.1 software package (Perkin-Elmer). For TEM, nodules were fixed with 3% glutaraldehyde (v/v) and 4% paraformaldehyde (v/v) in cacodylate buffer, postfixed in 1% osmium tetroxide, dehydrated in graded ethanol series, and embedded in LR White resin (London Resin). Serial 0.1-μm sections were cut with a diamond knife on a Leica EM UC7 ultramicrotome (Leica Microsystems). Ultrathin sections were then placed onto carbon coated copper grids and stained with 2% uranyl acetate followed by staining with Sato's lead (Sato, 1968). Specimens were observed under a Zeiss 10A (Carl Zeiss) transmission electron microscope operated at 80 kV. Images captured onto negative films were scanned and digitalized. All digital micrographs were processed using Adobe Photoshop CS4 (Adobe Systems).

Acetylene Reduction Assay

Acetylene reduction assays were performed according to the procedure of Oke and Long (1999). Plants were grown on a mixture of turface and vermiculite (2:1), watered with half-strength zero-nitrogen B&D solution, and inoculated with rhizobia *Sm1021*. At 15 dpi, entire root systems were dissected and placed into sealed 10-mL test tubes for the assays. Then 1 mL of air in each tube was replaced with acetylene to reach a concentration of 10% (v/v). Gas measurements (1 mL from each tube) were performed with an Agilent 7890A gas chromatograph (Agilent Technologies) after 18 to 24 h of incubation at 28°C.

Visualization of Iron in Nodule Cells

Imaging of Fe distribution in nodules of the wild-type and mutant plants was performed as described by Rodríguez-Haas et al. (2013). The Advanced Photon Source facility at Argonne National Laboratory was used to collect SXRF microspectrometry data.

Statistical Analysis

Statistical significance of observed differences was determined using one-way ANOVA and two-way ANOVA tests, with *P* value corrections for multiple

comparisons (posthoc tests). The analyses were run with Prism 7 software (GraphPad).

Accession Numbers

The CDS of *MtMATE67* from *M. truncatula* ecotype R108 is available from NCBI under accession number KP164499.

Supplemental Data

The following supplemental materials are available.

Supplemental Figure S1. *MtMATE67* is expressed predominantly in nodules.

Supplemental Figure S2. Homology model of MtMATE67.

Supplemental Figure S3. X-Gluc staining of mature nodules for *MtMATE67* (ecotype R108) promoter:GUS activity.

Supplemental Figure S4. Citrate uptake activity of negative control and *MtMATE67*-expressing *X. laevis* oocytes.

Supplemental Figure S5. Substrate selectivity of MtMATE67 measured by two-electrode voltage clamp.

Supplemental Figure S6. Transport activity of MtMATE67 for different organic acids.

Supplemental Figure S7. Untransformed negative control nodules stained in the same way as the HA-expressing nodules shown in Figure 5.

Supplemental Figure S8. Subcellular localization of MtMATE67-GFP fusion driven by the native or a constitutive promoter.

Supplemental Figure S9. Exon-intron structure of *MtMATE67* and positions of the *Tnt1* insertions in its genomic DNA isolated from ecotype R108.

Supplemental Figure S10. Time course of nodule development in wild-type (R108) and mutant (*mate67* line NF11278).

Supplemental Figure S11. *A. rhizogenes*-mediated genetic complementation of *mate67* mutant lines NF3177 and NF11278 with different versions of R108-derived *MtMATE67* CDS under a 3-kb native promoter.

Supplemental Figure S12. Electron micrographs of single infected cells from 10 dpi R108 wild-type nodules and *mate67* mutant (line NF11278) nodules.

Supplemental Figure S13. Microtome sections of R108 wild-type and *mate67* mutant nodules (line NF11278) 21 dpi.

Supplemental Figure S14. MtMATE67 contains a long cytosolic loop present in all plant MATE-type proteins shown to be associated with citrate transport.

Supplemental Table S1. Plant MATE transporters characterized by 2017.

Supplemental Table S2. *MtMATE67*-located homozygous *Tnt1* insertion in mutant lines NF3177 and NF11278 segregates in 3:1 ratio based on genotyping by PCR.

Supplemental Table S3. Expression of 13 *M. truncatula* symbiotic leghemoglobin genes, three nodule-expressed ferritin genes, and *MtMATE67* in different nodule zones.

Supplemental Table S4. Expression time course of eight *M. truncatula* leghemoglobin genes, three nodule-expressed ferritin genes, *Sinorhizobium meliloti NifH*, and *MtMATE67* in nodules, and their expression in different nodule zones/cell types, according to MtGEA v3.

Supplemental Table S5. List of primers and sequences used in this study.

Supplemental Data Set S1. Genomic DNA sequences, CDSs, and codon-optimized CDS of *MtMATE67*.

Supplemental Data Set S2. Alignment of the deduced amino acid sequences of MtMATE67 and 69 published plant proteins of MATE family (Excel format).

Supplemental Data Set S3. Alignment of the deduced amino acid sequences of MtMATE67 and 69 published plant proteins of MATE family (MEGA format).

Supplemental References. References for Supplemental Table S1.

ACKNOWLEDGMENTS

We thank Xiaofei Cheng and JiangQi Wen for their assistance with isolation of *Tnt1* mutants; Shulan Zhang for help with experiments; Frank Coker, Colleen Elles, Janie Gallaway, and Vicki Barrett for greenhouse support with *M. truncatula Tnt1* lines; and Mark Taylor for backcrossing the mutants. Pascal Ratet, Kirankumar S. Mysore, and Million Tadege are acknowledged for construction of the *Tnt1* mutant resource. We also thank Lina Yang for help with preparation of a high-resolution image for Figure 1. We appreciate the support from Jeremy Murray and Christopher Town with acquisition of genomic sequences. We also thank Jeremy Murray, Maria Harrison, Rebecca Dickstein, and Carroll Vance for data exchange and critical feedback.

Received October 24, 2017; accepted December 21, 2017; published December 28, 2017.

LITERATURE CITED

Appleby CA (1984) Leghemoglobin and rhizobium respiration. Annu Rev Plant Physiol **35:** 443–478

Benedito VA, Torres-Jerez I, Murray JD, Andriankaja A, Allen S, Kakar K, Wandrey M, Verdier J, Zuber H, Ott T, et al (2008) A gene expression atlas of the model legume *Medicago truncatula*. Plant J **55:** 504–513

Boisson-Dernier A, Chabaud M, Garcia F, Bécard G, Rosenberg C, Barker DG (2001) *Agrobacterium rhizogenes*-transformed roots of *Medicago truncatula* for the study of nitrogen-fixing and endomycorrhizal symbiotic associations. Mol Plant Microbe Interact **14:** 695–700

Boivin C, Camut S, Malpica CA, Truchet G, Rosenberg C (1990) *Rhizobium meliloti* genes encoding catabolism of trigonelline are induced under symbiotic conditions. Plant Cell **2:** 1157–1170

Bourcy M, Brocard L, Pislariu CI, Cosson V, Mergaert P, Tadege M, Mysore KS, Udvardi MK, Gourion B, Ratet P (2013) *Medicago truncatula* DNF2 is a PI-PLC-XD-containing protein required for bacteroid persistence and prevention of nodule early senescence and defense-like reactions. New Phytol **197:** 1250–1261

Brear EM, Day DA, Smith PM (2013) Iron: an essential micronutrient for the legume-rhizobium symbiosis. Front Plant Sci **4:** 359

Broughton WJ, Dilworth MJ (1971) Control of leghaemoglobin synthesis in snake beans. Biochem J **125:** 1075–1080

Brüggemann W, Maas-Kantel K, Moog P (1993) Iron uptake by leaf mesophyll cells: the role of the plasma membrane-bound ferric-chelate reductase. Planta **190:** 151–155

Cheng H-P, Walker GC (1998) Succinoglycan is required for initiation and elongation of infection threads during nodulation of alfalfa by *Rhizobium meliloti*. J Bacteriol **180:** 5183–5191

Cheng X, Wen J, Tadege M, Ratet P, Mysore KS (2011) Reverse genetics in *Medicago truncatula* using *Tnt1* insertion mutants. Methods Mol Biol **678:** 179–190

Conte SS, Walker EL (2011) Transporters contributing to iron trafficking in plants. Mol Plant **4:** 464–476

Curie C, Cassin G, Couch D, Divol F, Higuchi K, Le Jean M, Misson J, Schikora A, Czernic P, Mari S (2009) Metal movement within the plant: contribution of nicotianamine and yellow stripe 1-like transporters. Ann Bot **103:** 1–11

Durrett TP, Gassmann W, Rogers EE (2007) The FRD3-mediated efflux of citrate into the root vasculature is necessary for efficient iron translocation. Plant Physiol **144:** 197–205

Feng H, Xia X, Fan X, Xu G, Miller AJ (2013) Optimizing plant transporter expression in Xenopus oocytes. Plant Methods **9:** 48

Furukawa J, Yamaji N, Wang H, Mitani N, Murata Y, Sato K, Katsuhara M, Takeda K, Ma JF (2007) An aluminum-activated citrate transporter in barley. Plant Cell Physiol **48:** 1081–1091

Green LS, Rogers EE (2004) FRD3 controls iron localization in Arabidopsis. Plant Physiol **136:** 2523–2531

Guefrachi I, Nagymihaly M, Pislariu CI, Van de Velde W, Ratet P, Mars M, Udvardi MK, Kondorosi E, Mergaert P, Alunni B (2014) Extreme

specificity of NCR gene expression in *Medicago truncatula.* BMC Genomics **15:** 712

Hakoyama T, Niimi K, Watanabe H, Tabata R, Matsubara J, Sato S, Nakamura Y, Tabata S, Jichun L, Matsumoto T, et al (2009) Host plant genome overcomes the lack of a bacterial gene for symbiotic nitrogen fixation. Nature **462:** 514–517

Hakoyama T, Niimi K, Yamamoto T, Isobe S, Sato S, Nakamura Y, Tabata S, Kumagai H, Umehara Y, Brossuleit K, et al (2012) The integral membrane protein SEN1 is required for symbiotic nitrogen fixation in *Lotus japonicus* nodules. Plant Cell Physiol **53:** 225–236

Haney CH, Long SR (2010) Plant flotillins are required for infection by nitrogen-fixing bacteria. Proc Natl Acad Sci USA **107:** 478–483

Haynes JG, Czymmek KJ, Carlson CA, Veereshlingam H, Dickstein R, Sherrier JD (2004) Rapid analysis of legume root nodule development using confocal microscopy. New Phytol **163:** 661–668

He J, Benedito VA, Wang M, Murray JD, Zhao PX, Tang Y, Udvardi MK (2009) The *Medicago truncatula* gene expression atlas web server. BMC Bioinformatics **10:** 441

Hennecke H (1990) Nitrogen fixation genes involved in the *Bradyrhizobium japonicum*-soybean symbiosis. FEBS Lett **268:** 422–426

Hoover TR, Imperial J, Ludden PW, Shah VK (1989) Homocitrate is a component of the iron-molybdenum cofactor of nitrogenase. Biochemistry **28:** 2768–2771

Jeong J, Guerinot ML (2009) Homing in on iron homeostasis in plants. Trends Plant Sci **14:** 280–285

Kaiser BN, Moreau S, Castelli J, Thomson R, Lambert A, Bogliolo S, Puppo A, Day DA (2003) The soybean NRAMP homologue, GmDMT1, is a symbiotic divalent metal transporter capable of ferrous iron transport. Plant J **35:** 295–304

Kakar K, Wandrey M, Czechowski T, Gaertner T, Scheible WR, Stitt M, Torres-Jerez I, Xiao Y, Redman JC, Wu HC, et al (2008) A community resource for high-throughput quantitative RT-PCR analysis of transcription factor gene expression in *Medicago truncatula.* Plant Methods **4:** 18

Karimi M, Inzé D, Depicker A (2002) GATEWAY vectors for *Agrobacterium*-mediated plant transformation. Trends Plant Sci **7:** 193–195

Kobayashi T, Nishizawa NK (2012) Iron uptake, translocation, and regulation in higher plants. Annu Rev Plant Biol **63:** 131–152

Kochian LV, Piñeros MA, Liu J, Magalhaes JV (2015) Plant adaptation to acid soils: the molecular basis for crop aluminum resistance. Annu Rev Plant Biol **66:** 571–598

Krieg PA, Melton DA (1984) Functional messenger RNAs are produced by SP6 in vitro transcription of cloned cDNAs. Nucleic Acids Res **12:** 7057–7070

Kryvoruchko IS, Sinharoy S, Torres-Jerez I, Sosso D, Pislariu CI, Guan D, Murray J, Benedito VA, Frommer WB, Udvardi MK (2016) MtSWEET11, a nodule-specific sucrose transporter of *Medicago truncatula.* Plant Physiol **171:** 554–565

Kumar S, Stecher G, Tamura K (2016) MEGA7: Molecular Evolutionary Genetics Analysis version 7.0 for bigger datasets. Mol Biol Evol **33:** 1870–1874

LeVier K, Day DA, Guerinot ML (1996) Iron uptake by symbiosomes from soybean root nodules. Plant Physiol **111:** 893–900

Liu J, Magalhaes JV, Shaff J, Kochian LV (2009) Aluminum-activated citrate and malate transporters from the MATE and ALMT families function independently to confer Arabidopsis aluminum tolerance. Plant J **57:** 389–399

Lu M (2016) Structures of multidrug and toxic compound extrusion transporters and their mechanistic implications. Channels (Austin) **10:** 88–100

Maróti G, Kondorosi E (2014) Nitrogen-fixing Rhizobium-legume symbiosis: are polyploidy and host peptide-governed symbiont differentiation general principles of endosymbiosis? Front Microbiol **5:** 326

Meyer S, De Angeli A, Fernie AR, Martinoia E (2010) Intra- and extracellular excretion of carboxylates. Trends Plant Sci **15:** 40–47

Moreau S, Meyer J-M, Puppo A (1995) Uptake of iron by symbiosomes and bacteroids from soybean nodules. FEBS Lett **361:** 225–228

Moriyama Y, Hiasa M, Matsumoto T, Omote H (2008) Multidrug and toxic compound extrusion (MATE)-type proteins as anchor transporters for the excretion of metabolic waste products and xenobiotics. Xenobiotica **38:** 1107–1118

Murray JD (2011) Invasion by invitation: rhizobial infection in legumes. Mol Plant Microbe Interact **24:** 631–639

Nakagawa T, Kurose T, Hino T, Tanaka K, Kawamukai M, Niwa Y, Toyooka K, Matsuoka K, Jinbo T, Kimura T (2007) Development of series of gateway binary vectors, pGWBs, for realizing efficient construction of fusion genes for plant transformation. J Biosci Bioeng **104:** 34–41

O'Hara GW (2001) Nutritional constraints on root nodule bacteria affecting symbiotic nitrogen fixation: a review. Aust J Exp Agric **41:** 417–433

Oke V, Long SR (1999) Bacterial genes induced within the nodule during the Rhizobium-legume symbiosis. Mol Microbiol **32:** 837–849

Oldroyd GE (2013) Speak, friend, and enter: signalling systems that promote beneficial symbiotic associations in plants. Nat Rev Microbiol **11:** 252–263

Omote H, Hiasa M, Matsumoto T, Otsuka M, Moriyama Y (2006) The MATE proteins as fundamental transporters of metabolic and xenobiotic organic cations. Trends Pharmacol Sci **27:** 587–593

Ott T, van Dongen JT, Günther C, Krusell L, Desbrosses G, Vigeolas H, Bock V, Czechowski T, Geigenberger P, Udvardi MK (2005) Symbiotic leghemoglobins are crucial for nitrogen fixation in legume root nodules but not for general plant growth and development. Curr Biol **15:** 531–535

Peoples MB, Brockwell J, Herridge DF, Rochester IJ, Alves BJR, Urquiaga S, Boddey RM, Dakora FD, Bhattarai S, Maskey SL, et al (2009) The contributions of nitrogen-fixing crop legumes to the productivity of agricultural systems. Symbiosis **48:** 1–17

Pislariu CI, Dickstein R (2007) An IRE-like AGC kinase gene, *MtIRE*, has unique expression in the invasion zone of developing root nodules in *Medicago truncatula.* Plant Physiol **144:** 682–694

Quandt HJ, Pühler A, Broer I (1993) Transgenic root nodules of *Vicia hirsuta*: a fast and efficient system for the study of gene expression in indeterminate-type nodules. Mol Plant Microbe Interact **6:** 699–706

Rellán-Alvarez R, Giner-Martínez-Sierra J, Orduna J, Orera I, Rodríguez-Castrillón JA, García-Alonso JI, Abadía J, Alvarez-Fernández A (2010) Identification of a tri-iron(III), tri-citrate complex in the xylem sap of iron-deficient tomato resupplied with iron: new insights into plant iron long-distance transport. Plant Cell Physiol **51:** 91–102

Rodríguez-Haas B, Finney L, Vogt S, González-Melendi P, Imperial J, González-Guerrero M (2013) Iron distribution through the developmental stages of *Medicago truncatula* nodules. Metallomics **5:** 1247–1253

Roschzttardtz H, Séguéla-Arnaud M, Briat JF, Vert G, Curie C (2011) The FRD3 citrate effluxer promotes iron nutrition between symplastically disconnected tissues throughout Arabidopsis development. Plant Cell **23:** 2725–2737

Roux B, Rodde N, Jardinaud MF, Timmers T, Sauviac L, Cottret L, Carrère S, Sallet E, Courcelle E, Moreau S, et al (2014) An integrated analysis of plant and bacterial gene expression in symbiotic root nodules using laser-capture microdissection coupled to RNA sequencing. Plant J **77:** 817–837

Sato T (1968) A modified method for lead staining of thin sections. J Electron Microsc (Tokyo) **17:** 158–159

Shoji T (2014) ATP-binding cassette and multidrug and toxic compound extrusion transporters in plants: a common theme among diverse detoxification mechanisms. Int Rev Cell Mol Biol **309:** 303–346

Silva AMN, Kong X, Parkin MC, Cammack R, Hider RC (2009) Iron(III) citrate speciation in aqueous solution. Dalton Trans (40): 8616–8625

Sinharoy S, Torres-Jerez I, Bandyopadhyay K, Kereszt A, Pislariu CI, Nakashima J, Benedito VA, Kondorosi E, Udvardi MK (2013) The C2H2 transcription factor regulator of symbiosome differentiation represses transcription of the secretory pathway gene *VAMP721a* and promotes symbiosome development in *Medicago truncatula.* Plant Cell **25:** 3584–3601

Suganuma N, Nakamura Y, Yamamoto M, Ohta T, Koiwa S, Kawaguchi M (2003) The *Lotus japonicus* Sen1 gene controls rhizobial differentiation into nitrogen-fixing bacteroids in nodules. Mol Genet Genomics **269:** 312–320

Tadege M, Wen J, He J, Tu H, Kwak Y, Eschstruth A, Cayrel A, Endre G, Zhao PX, Chabaud M, et al (2008) Large-scale insertional mutagenesis using the *Tnt1* retrotransposon in the model legume *Medicago truncatula.* Plant J **54:** 335–347

Takanashi K, Shitan N, Yazaki K (2014) The Multidrug and Toxic Compound Extrusion (MATE) family in plants. Plant Biotechnol **31:** 417–430

Takanashi K, Yokosho K, Saeki K, Sugiyama A, Sato S, Tabata S, Ma JF, Yazaki K (2013) LjMATE1: a citrate transporter responsible for iron supply to the nodule infection zone of *Lotus japonicus.* Plant Cell Physiol **54:** 585–594

Tang C, Robson AD, Dilworth MJ (1990) The role of iron in nodulation and nitrogen fixation in *Lupinus angustifolius* L. New Phytol **114:** 173–182

Tang H, Krishnakumar V, Bidwell S, Rosen B, Chan A, Zhou S, Gentzbittel L, Childs KL, Yandell M, Gundlach H, Mayer KF, Schwartz DC, et al (2014) An improved genome release (version Mt4.0) for the model legume *Medicago truncatula.* BMC Genomics **15:** 312

Taylor M, Blaylock L, Nakashima J, McAbee D, Ford J, Harrison M, Udvardi M (2011) *Medicago truncatula* hybridization: supplemental videos. *In* U Mathesius, EP Journet, LW Sumner LW, eds, *Medicago truncatula* Handbook, Version July 2011. Noble Research Institute, Ardmore, OK, pp 1–55

Tejada-Jiménez M, Castro-Rodríguez R, Kryvoruchko I, Lucas MM, Udvardi M, Imperial J, González-Guerrero M (2015) *Medicago truncatula* natural resistance-associated macrophage Protein1 is required for iron uptake by rhizobia-infected nodule cells. Plant Physiol **168:** 258–272

Terpolilli JJ, Hood GA, Poole PS (2012) What determines the efficiency of $N_{(2)}$-fixing Rhizobium-legume symbioses? Adv Microb Physiol **60:** 325–389

Timmers AC, Auriac MC, Truchet G (1999) Refined analysis of early symbiotic steps of the Rhizobium-Medicago interaction in relationship with microtubular cytoskeleton rearrangements. Development **126:** 3617–3628

Udvardi M, Poole PS (2013) Transport and metabolism in legume-rhizobia symbioses. Annu Rev Plant Biol **64:** 781–805

Vasse J, de Billy F, Camut S, Truchet G (1990) Correlation between ultrastructural differentiation of bacteroids and nitrogen fixation in alfalfa nodules. J Bacteriol **172:** 4295–4306

Veerappan V, Kadel K, Alexis N, Scott A, Kryvoruchko I, Sinharoy S, Taylor M, Udvardi M, Dickstein R (2014) Keel petal incision: a simple and efficient method for genetic crossing in *Medicago truncatula.* Plant Methods **10:** 11

Vincill ED, Szczyglowski K, Roberts DM (2005) GmN70 and LjN70. Anion transporters of the symbiosome membrane of nodules with a transport preference for nitrate. Plant Physiol **137:** 1435–1444

Wang J, Hou Q, Li P, Yang L, Sun X, Benedito VA, Wen J, Chen B, Mysore KS, Zhao J (2017) Diverse functions of multidrug and toxin extrusion (MATE) transporters in citric acid efflux and metal homeostasis in *Medicago truncatula.* Plant J **90:** 79–95

Yokosho K, Yamaji N, Ma JF (2011) An Al-inducible MATE gene is involved in external detoxification of Al in rice. Plant J **68:** 1061–1069